

Singlet Model Interference Effects with High Scale UV Physics

S. Dawson^a and I. M. Lewis^b

^a*Department of Physics, Brookhaven National Laboratory, Upton, N.Y., 11973 USA*

^b*Department of Physics and Astronomy, University of Kansas, Lawrence, Kansas, 66045 USA*

(Dated: October 19, 2016)

Abstract

One of the simplest extensions of the Standard Model (SM) is the addition of a scalar gauge singlet, S . If S is not forbidden by a symmetry from mixing with the Standard Model Higgs boson, the mixing will generate non-SM rates for Higgs production and decays. In general, there could also be unknown high energy physics that generates additional effective low energy interactions. We show that interference effects between the scalar resonance of the singlet model and the effective field theory (EFT) operators can have significant effects in the Higgs sector. We examine a non- Z_2 symmetric scalar singlet model and demonstrate that a fit to the 125 GeV Higgs boson couplings and to limits on high mass resonances, S , exhibit an interesting structure and possible large cancellations of effects between the resonance contribution and the new EFT interactions, that invalidate conclusions based on the renormalizable singlet model alone.

I. INTRODUCTION

Among the simplest extensions of the Standard Model (SM) is the addition of a gauge singlet scalar particle, S . The singlet particle couples to SM particles through its mixing with the SM-like 125 GeV Higgs boson. In general, there can be additional interactions between the S and the gauge bosons, which can be parameterized as effective field theory (EFT) dimension-5 couplings. The source of these effective interactions is not relevant for our discussion and our focus is on the consequences of the interference effects between the heavy scalar resonance and the EFT operators. Since there are a relatively few number of EFT operators coupling the singlet to the $SU(3) \times SU(2) \times U(1)$ gauge bosons, it is possible to obtain interesting limits on the theory, despite the addition of new parameters.

In the absence of a Z_2 symmetry, the singlet model allows cubic and linear self-coupling terms in the scalar potential and a strong first order electroweak phase transition is possible for certain values of the parameter space[1–5], making this theory highly motivated phenomenologically. We begin by examining restrictions on the parameters of the non- Z_2 symmetric model from the measured 125 GeV Higgs couplings and from the requirement that the electroweak minimum be the absolute minima of the potential. We then include LHC limits on heavy resonances that decay into SM particles (assuming that there are no additional light particles). Novel features of our analysis are the insistence that the parameters satisfy the minimization condition of the potential and our inclusion of interference effects between the SM contributions to the Higgs widths and the contributions from the EFT interactions. These interference effects can be large and significantly change the allowed regions of parameter space.

In Sec. II, we review the singlet model and the EFT interactions, along with compact expressions for the decay widths. Sec. III discusses constraints from the 125 GeV Higgs, and Sec. IV contains our limits on the properties of both the 125 scalar and EFT coefficients, and a discussion of the size of the allowed mixing between the SM-like and heavy scalars in the presence of EFT coefficients. Section V contains some conclusions.

II. MODEL CONSIDERATIONS

A. Singlet plus EFT Model

We consider a model containing the SM Higgs doublet, H , and an additional scalar singlet, S . The most general renormalizable scalar potential is,

$$V(H, S) = -\mu^2 H^\dagger H + \lambda(H^\dagger H)^2 + \frac{a_1}{2} H^\dagger H S + \frac{a_2}{2} H^\dagger H S^2 + b_1 S + \frac{b_2}{2} S^2 + \frac{b_3}{3} S^3 + \frac{b_4}{4} S^4. \quad (1)$$

The singlet model has been examined in some detail in the literature[1, 2, 6–12] and so our discussion is appropriately brief. If there is a Z_2 symmetry $S \rightarrow -S$, then $a_1 = b_1 = b_3 = 0$. The Z_2 non-symmetric model is, however, particularly interesting since it is possible to arrange the parameters in such a way as to obtain a strong first order phase transition[1–5, 13].

The neutral scalar components of the doublet H and singlet S are denoted by $\phi_0 = (h+v)/\sqrt{2}$ and $S = s+x$, where the vacuum expectation values are $\langle\phi_0\rangle = \frac{v}{\sqrt{2}}$ and $\langle S\rangle = x$. We require that the global minimum of the potential correspond to the electroweak symmetry breaking (EWSB) minimum, $v = v_{EW} = 246$ GeV[1, 9], which places significant constraints on the allowed parameters. Note that a shift of the singlet field by $S \rightarrow S + \Delta_S$ is just a redefinition of the parameters of Eq. 1 and we are free to choose our electroweak symmetry breaking minimum as $(v, x) \equiv (v_{EW}, 0)$ ¹.

The physical scalars are mixtures of h and s , and the scalar mixing is parameterized as,

$$\begin{pmatrix} h_1 \\ h_2 \end{pmatrix} = \begin{pmatrix} \cos \theta & \sin \theta \\ -\sin \theta & \cos \theta \end{pmatrix} \begin{pmatrix} h \\ s \end{pmatrix}, \quad (2)$$

where $h_{1,2}$ are the mass eigenstates with masses m_1, m_2 . The parameters of the scalar

¹ This freedom to set $x = 0$ does not occur in the Z_2 symmetric case.

potential can be solved for in terms of the physical masses and mixing,

$$\begin{aligned}
a_1 &= \frac{m_1^2 - m_2^2}{v} \sin 2\theta, \\
b_2 + \frac{a_2}{2} v^2 &= m_1^2 \sin^2 \theta + m_2^2 \cos^2 \theta, \\
\lambda &= \frac{m_1^2 \cos^2 \theta + m_2^2 \sin^2 \theta}{2v^2} \\
\mu^2 &= \lambda v^2 \\
b_1 &= -\frac{v^2}{4} a_1.
\end{aligned} \tag{3}$$

Our free parameters are then,

$$m_1 = 125 \text{ GeV}, \quad m_2, \quad \theta, \quad v_{EW} = 246 \text{ GeV}, \quad x = 0, \quad a_2, \quad b_3, \quad b_4. \tag{4}$$

The couplings of the h_1 to SM particles are suppressed by $\cos \theta$ and both ATLAS and CMS have obtained limits from the measured couplings. ATLAS finds at 95% confidence level, $\sin \theta \leq .35$, assuming no branching ratio to invisible particles[14]. Using the fitted global signal strength for the SM Higgs boson, $\mu = 1.03_{-0.15}^{+0.17}$ [15], a 95% confidence level limit can be extracted, $\sin \theta \leq .51$. In the absence of the EFT coefficients, a fit to the oblique parameters also restricts $\sin \theta$ [2, 8, 9, 16], but the limit from Higgs coupling measurements is stronger.

The limits on $\sin \theta$ can be significantly altered, however, when the EFT operators are included. We postulate the $SU(3) \times SU(2) \times U(1)$ gauge invariant effective interactions,

$$L = g_s^2 \frac{c_{gg}}{\Lambda} S G^{\mu\nu, A} G_{\mu\nu}^A + \frac{c_{WW}}{\Lambda} g^2 S W^{\mu\nu, a} W_{\mu\nu}^a + \frac{c_{BB}}{\Lambda} g'^2 S B^{\mu\nu} B_{\mu\nu}, \tag{5}$$

that are assumed to arise from unknown UV physics at a scale Λ . The scalar couplings to gauge bosons are suppressed by the appropriate factor of $\cos \theta$ or $\sin \theta$ and receive additional contributions from the interactions of Eq. 5. There is an interplay of effects between the singlet-SM mixing of Eq. 2 and the EFT contributions from Eq. 5, which requires that we fit the data to the complete model[17, 18].

Finally, we need the self-interactions of the Higgs bosons in the basis of the mass eigenstates h_1 and h_2 ,

$$V_{\text{self}} \supset \frac{\lambda_{111}}{3!} h_1^3 + \frac{\lambda_{211}}{2!} h_2 h_1^2 + \dots \tag{6}$$

where[8, 9],

$$\begin{aligned}
\lambda_{111} &= 2s_\theta^3 b_3 + \frac{3a_1}{2} s_\theta c_\theta^2 + 3a_2 s_\theta^2 c_\theta v + 6c_\theta^3 \lambda v, \\
\lambda_{211} &= 2s_\theta^2 c_\theta b_3 + \frac{a_1}{2} c_\theta (c_\theta^2 - 2s_\theta^2) + (2c_\theta^2 - s_\theta^2) s_\theta v a_2 - 6\lambda s_\theta c_\theta^2 v.
\end{aligned} \tag{7}$$

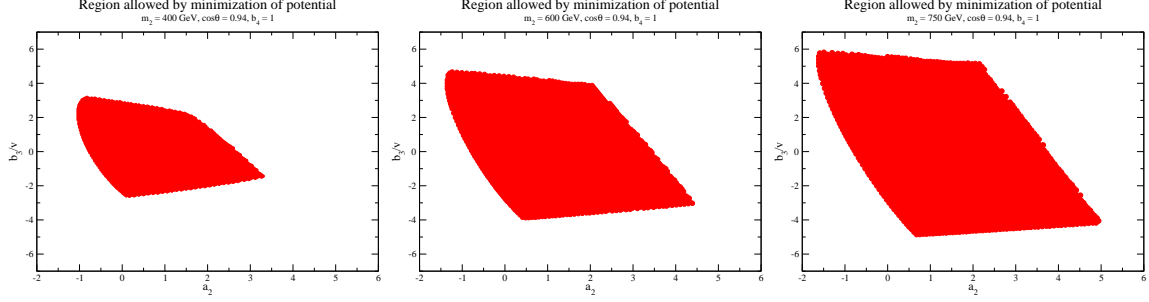


FIG. 1: Regions allowed by the requirement that the electroweak minimum be a global minimum for $\cos\theta = 0.94$, $b_4 = 1$ and $m_2 = 400, 600$, and 750 GeV[9].

and we abbreviate $s_\theta = \sin\theta$, $c_\theta = \cos\theta$ and assume $\sin\theta > 0$. In the small angle limit, to $\mathcal{O}(s_\theta^2)$,

$$\lambda_{111} \rightarrow 6\lambda v + \frac{3}{2}a_1 s_\theta + 3v s_\theta^2(a_2 - 3\lambda) \quad (8)$$

$$\begin{aligned} &\sim \frac{3m_1^2}{v} + s_\theta^2 \frac{3}{2v} (m_2^2 - 4m_1^2 + 2a_2 v^2) \\ \lambda_{211} &\rightarrow \frac{a_1}{2} + s_\theta v(-6\lambda + 2a_2) + \frac{s_\theta^2}{4}(8b_3 - 7a_1) \\ &\sim s_\theta \left(-\frac{3m_1^2}{v} + 2va_2 \right) + \frac{s_\theta c_\theta}{2v} (m_1^2 - m_2^2) + 2b_3 s_\theta^2. \end{aligned} \quad (9)$$

The restrictions on the parameters of the potential due to the requirement that the electroweak minimum be a global minimum were examined in Ref. [1, 9]. In Fig. 1, we fix $b_4 = 1$, $\cos\theta = .94$ and show the allowed regions for a_2 and b_3 for different values of the heavy scalar mass, m_2 . The areas of these regions increase with b_4 and the edges of the contours are completely fixed by the global minimum requirement as described in Ref. [9]². The regions become somewhat larger as m_2 increases for fixed b_4 . In the softly broken Z_2 scenario of Ref. [5], a first order electroweak phase transition requires $a_2 > \sim 9$. In the model without a Z_2 symmetry, a strong first order electroweak phase transition appears to be possible for $a_2 \sim 1 - 2$, and negative b_3 [3], although the maximum m_2 studied in this reference is 250 GeV.

The partial width of $h_2 \rightarrow h_1 h_1$ is,

$$\Gamma(h_2 \rightarrow h_1 h_1) = \frac{\lambda_{211}^2}{32\pi m_2} \sqrt{1 - \frac{4m_1^2}{m_2^2}}. \quad (10)$$

² *i.e.* all points within the shaded regions are allowed by the minimization of the potential.

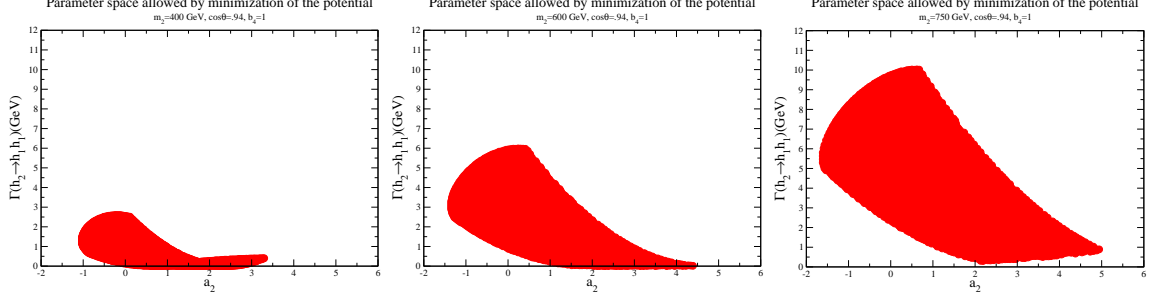


FIG. 2: Allowed decay widths for $h_2 \rightarrow h_1 h_1$ assuming the parameters correspond to a global minimum of the potential for $b_4 = 1$, $\cos \theta = 0.94$, and $m_2 = 400, 600$ and 750 GeV .

In Fig. 2 we show the partial widths for $h_2 \rightarrow h_1 h_1$ using the allowed values of b_3 from Fig. 1 for each parameter point for representative values of the parameters. The width can potentially increase significantly as the resonance mass increases. A measurement of the coupling λ_{211} to sufficient precision could shed light on the values of a_2 and b_3 . We note that in all cases, $\Gamma(h_2 \rightarrow h_1 h_1)_{\max}/m_2 \sim 1\%$, and so we are in a narrow width scenario.

B. Results for Decay widths

The decays of h_1 and h_2 are affected by the SM doublet-singlet mixing and by the EFT operators. Retaining the interference with the SM contributions, we find for the heavier state:

$$\begin{aligned}
 \Gamma(h_2 \rightarrow \gamma\gamma) &= \frac{e^4 m_2^3}{4\pi} \left| \sin \theta \left(\frac{\sum_i N_{ci} e_i^2 F_i(\tau_{2i})}{32\pi^2 v} \right) + \cos \theta \frac{c_{\gamma\gamma}}{\Lambda} \right|^2 \\
 \Gamma(h_2 \rightarrow gg) &= \frac{2g_s^4 m_2^3}{\pi} \left| \sin \theta \frac{\sum_i F_i(\tau_{2i})}{64\pi^2 v} + \cos \theta \frac{c_{gg}}{\Lambda} \right|^2 \\
 \Gamma(h_2 \rightarrow ZZ) &= \frac{1}{32\pi} \frac{m_2^3}{v^2} \sqrt{1 - 4x_{2Z}} \left\{ 2^7 \cos^2 \theta \frac{c_{ZZ}^2 M_Z^4}{\Lambda^2 v^2} (1 - 4x_{2Z} + 6x_{2Z}^2) \right. \\
 &\quad \left. + 3 \cdot 2^5 \cos \theta \sin \theta \frac{c_{ZZ} M_Z^2}{v\Lambda} x_{2Z} (1 - 2x_{2Z}) + \sin^2 \theta (1 - 4x_{2Z} + 12x_{2Z}^2) \right\} \\
 \Gamma(h_2 \rightarrow Z\gamma) &= \frac{e^4 m_2^3}{2\pi s_W^2 c_W^2} (1 - x_{2Z})^3 \left| \sin \theta \frac{c_W s_W}{32\pi^2 v} (A_F + A_W) - \cos \theta \frac{c_{Z\gamma}}{\Lambda} \right|^2 \\
 \Gamma(h_2 \rightarrow W^+ W^-) &= \frac{1}{16} \frac{m_2^3}{\pi v^2} \sqrt{1 - 4x_{2W}} \left\{ 2^7 \cos^2 \theta \frac{c_{WW}^2 M_W^4}{\Lambda^2 v^2} (1 - 4x_{2W} + 6x_{2W}^2) \right. \\
 &\quad \left. + 3 \cdot 2^5 \cos \theta \sin \theta \frac{c_{WW} M_W^2}{v\Lambda} x_{2W} (1 - 2x_{2W}) + \sin^2 \theta (1 - 4x_{2W} + 12x_{2W}^2) \right\} \\
 \Gamma(h_2 \rightarrow f\bar{f}) &= \sin^2 \theta \Gamma(h \rightarrow f\bar{f})_{SM}, \tag{11}
 \end{aligned}$$

where [19–21],

$$\begin{aligned}
F_i(\tau_{2i}) &= -2\tau_{2i} \left(1 + (1 - \tau_{2i})f(\tau_{2i}) \right) \text{ for fermions} \\
F_W(\tau_{2W}) &= 2 + 3\tau_{2W} + 3\tau_{2W}(2 - \tau_{2W})f(\tau_{2W}) \text{ for gauge bosons} \\
x_{iV} &= \frac{M_V^2}{m_i^2} \\
c_{\gamma\gamma} &= c_{WW} + c_{BB} \\
c_{ZZ} &= c_W^4 c_{WW} + s_W^4 c_{BB} \\
c_{Z\gamma} &= c_{BB}s_W^2 - c_{WW}c_W^2,
\end{aligned} \tag{12}$$

and e_i is the electric charge of particle i , $c_W = M_W/M_Z$, $N_{ci} = 3(1)$ for quarks (leptons), $\tau_{2i} = \frac{4M_i^2}{m_2^2}$, M_i is the mass of the appropriate fermion or the W boson, A_F and A_W are given in Ref.[19], and

$$\begin{aligned}
f(\tau) &= \left[\sin^{-1} \left(\frac{1}{\sqrt{\tau}} \right) \right]^2, \quad \text{if } \tau \geq 1 \\
&= -\frac{1}{4} \left[\ln \left(\frac{1+\sqrt{1-\tau}}{1-\sqrt{1-\tau}} \right) - i\pi \right]^2 \quad \text{if } \tau < 1.
\end{aligned} \tag{13}$$

If we consider a model with no mixing with the SM Higgs, $\sin \theta = 0$, we have approximately,

$$\begin{aligned}
\Gamma(h_2 \rightarrow \gamma\gamma) &= .04 c_{\gamma\gamma}^2 \left(\frac{m_2}{600 \text{ GeV}} \right)^3 \left(\frac{2 \text{ TeV}}{\Lambda(\text{TeV})} \right)^2 \text{ GeV} \\
\Gamma(h_2 \rightarrow W^+W^-) &= 0.15 c_{WW}^2 \left(\frac{m_2}{600 \text{ GeV}} \right)^3 \left(\frac{2 \text{ TeV}}{\Lambda(\text{TeV})} \right)^2 \text{ GeV} \\
\Gamma(h_2 \rightarrow ZZ) &= 1.2 c_{ZZ}^2 \left(\frac{m_2}{600 \text{ GeV}} \right)^3 \left(\frac{2 \text{ TeV}}{\Lambda(\text{TeV})} \right)^2 \text{ GeV} \\
\Gamma(h_2 \rightarrow Z\gamma) &= 0.43 c_{Z\gamma}^2 \left(\frac{m_2}{600 \text{ GeV}} \right)^3 \left(\frac{2 \text{ TeV}}{\Lambda(\text{TeV})} \right)^2 \text{ GeV}.
\end{aligned} \tag{14}$$

Note that Eq. 14 is an over-constrained result due to the relations of Eq. 12.

The lighter Higgs boson ($m_1 = 125 \text{ GeV}$) decay widths are,

$$\begin{aligned}
\Gamma(h_1 \rightarrow gg) &= \frac{2g_s^4 m_1^3}{\pi} \left| -\cos\theta \frac{\sum_i F_i(\tau_{1i})}{64\pi^2 v} + \sin\theta \frac{c_{gg}}{\Lambda} \right|^2 \\
\Gamma(h_1 \rightarrow \gamma\gamma) &= \frac{e^4 m_1^3}{4\pi} \left| -\cos\theta \left(\frac{\sum_i N_{ci} e_i^2 F_i(\tau_{1i})}{32\pi^2 v} \right) + \sin\theta \frac{c_{\gamma\gamma}}{\Lambda} \right|^2 \\
\Gamma(h_1 \rightarrow WW^*) &= \frac{18g^2 M_W^4}{\pi^3 v^2 m_1} \left\{ \sin^2\theta \frac{c_{WW}^2}{v^2 \Lambda^2} m_1^4 I_3(M_W) - \cos\theta \sin\theta \frac{c_{WW}}{4v\Lambda} m_1^2 I_2(M_W) + \frac{1}{64} \cos^2\theta I_1(M_W) \right\} \\
\Gamma(h_1 \rightarrow ZZ^*) &= \kappa \frac{2g^2 M_Z^4}{c_W^2 \pi^3 v^2 m_1} \left\{ \sin^2\theta \frac{c_{ZZ}^2}{v^2 \Lambda^2} m_1^4 I_3(M_Z) - \cos\theta \sin\theta \frac{c_{ZZ}}{4v\Lambda} m_1^2 I_2(M_Z) + \frac{1}{64} \cos^2\theta I_1(M_Z) \right\} \\
\Gamma(h_1 \rightarrow Z\gamma) &= \frac{e^4 m_1^3}{2\pi s_W^2 c_W^2} (1 - x_{1Z})^3 \left| \cos\theta \frac{c_W s_W}{32\pi^2 v} (A_F + A_W) + \sin\theta \frac{c_{Z\gamma}}{\Lambda} \right|^2 \\
\Gamma(h_1 \rightarrow f\bar{f}) &= \cos^2\theta \Gamma(h \rightarrow f\bar{f})_{SM}
\end{aligned} \tag{15}$$

where,

$$\begin{aligned}
I_1(M_W) &= \int_0^{(m_1 - M_W)^2} dq^2 \frac{q^2}{m_1^2} \left(1 + \frac{1}{3} \frac{\hat{\lambda}(m_1^2, M_W^2, q^2)}{4q^2 M_W^2} \right) \frac{\hat{\lambda}^{1/2}(m_1^2, M_W^2, q^2)}{(q^2 - M_W^2)^2 + \Gamma_W^2 M_W^2} \\
I_2(M_W) &= \int_0^{(m_1 - M_W)^2} dq^2 \frac{q^2}{m_1^2} \frac{M_1^2 - M_W^2 - q^2}{2m_1^2} \frac{\hat{\lambda}^{1/2}(m_1^2, M_W^2, q^2)}{(q^2 - M_W^2)^2 + \Gamma_W^2 M_W^2} \\
I_3(M_W) &= \int_0^{(m_1 - M_W)^2} dq^2 \frac{q^2}{m_1^2} \frac{3(m_1^2 - M_W^2 - q^2)^2 - \hat{\lambda}(m_1^2, M_W^2, q^2)}{12m_1^4} \frac{\hat{\lambda}^{1/2}(m_1^2, M_W^2, q^2)}{(q^2 - M_W^2)^2 + \Gamma_W^2 M_W^2} \\
\hat{\lambda}(x, y, z) &= (x - y - z)^2 - 4yz,
\end{aligned} \tag{16}$$

$\tau_{1i} = \frac{4M_i^2}{m_1^2}$, the coefficient κ is,

$$\begin{aligned}
\kappa &= 3\left(\frac{1}{2} - s_W^2\right)^2 + s_W^4 + 3N_c\left(-\frac{1}{2} + \frac{1}{3}s_W^2\right)^2 + \frac{1}{9}s_W^4 + 2N_c\left(\left(\frac{1}{2} - \frac{2}{3}s_W^2\right)^2 + \frac{4}{9}s_W^4\right) \\
&= 3.68,
\end{aligned} \tag{17}$$

with $N_c = 3$ and $s_W^2 = \sin^2\theta_W = 1 - \frac{M_W^2}{M_Z^2}$.

Some typical branching ratios of h_1 into WW and ZZ normalized to the SM are shown in Fig. 3, and demonstrate little sensitivity to either c_{BB} or c_{WW} with sub-percent level deviations. The branching ratios to $\gamma\gamma$ and $Z\gamma$ are shown in Fig. 4 and are very sensitive to c_{WW} and c_{BB} , changing upwards of 50% from the SM values. This is due to the SM rate first occurring at one loop. We note that in the limit $c_{gg} = c_{WW} = c_{BB} = 0$, all of the branching ratios are equal to their SM values for $\sin\theta = 0$, and the deviations from 1 in Figs. 3 and 4 are a result of the interplay between the singlet mixing and the EFT operators. These figures retain only the linear terms in the EFT couplings, as we have implicitly assumed s_θ

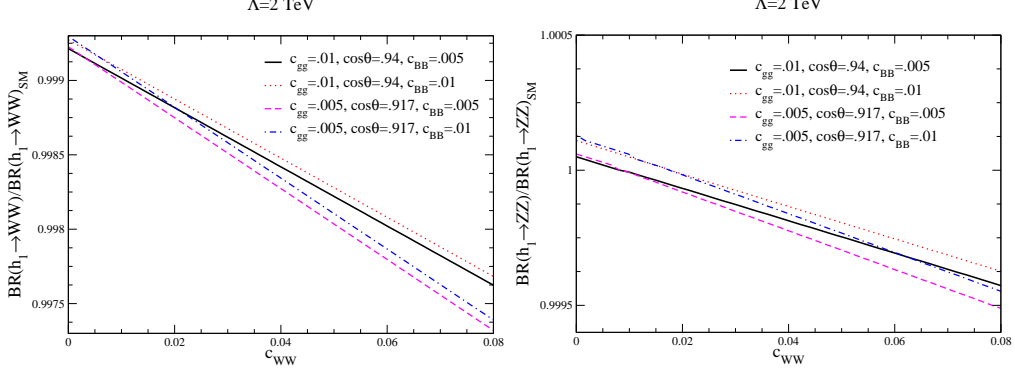


FIG. 3: Branching ratio for (LHS) $h_1 \rightarrow WW$, and (RHS) $h_1 \rightarrow ZZ$ for representative values of the parameters.

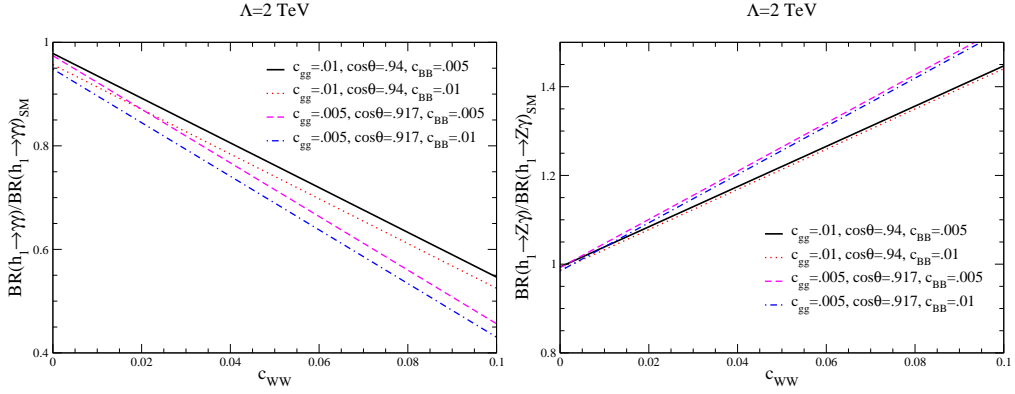


FIG. 4: Branching ratios for (LHS) $h_1 \rightarrow \gamma\gamma$, and (RHS) $h_1 \rightarrow Z\gamma$ for representative values of the parameters.

is small and we note that the c_i^2 coefficients are always suppressed by s_θ^2 for h_1 production (see Eq. 15).

For completeness, we note that the hadronic cross section for production of h_1 or h_2 from gluon fusion is,

$$\sigma(pp \rightarrow h_i) = \frac{\pi^2}{8m_i S_H} \Gamma(h_i \rightarrow gg) L \quad (18)$$

where

$$L = \int_{\ln(\sqrt{\zeta})}^{-\ln(\sqrt{\zeta})} dy g(\sqrt{\zeta} e^y) g(\sqrt{\zeta} e^{-y}), \quad (19)$$

$\sqrt{S_H}$ is the hadronic center-of-mass energy and $\zeta = m_i^2/S_H$.

III. CONSTRAINTS FROM h_1

The measurements of SM Higgs couplings place stringent restrictions on the allowed parameters of the model. Both ATLAS and CMS limit the mixing angle, θ , in the singlet model in the case $c_{gg} = c_{WW} = c_{BB} = 0$, as discussed in the previous section. These limits are significantly effected by the addition of the EFT operators. We fit to the parameters of our model using the combined ATLAS/CMS 8 *TeV* results[15]. The simplest possible limit is obtained by a fit to the over-all gluon fusion signal strength for h_1 ,

$$\mu_{ggF} = 1.03^{+.17}_{-.15}. \quad (20)$$

The 95% confidence level limit from the ggF signal strength is shown in Fig. 5. This fit demonstrates the cancellations between the contributions of the singlet model and the contributions of the EFT coefficients. For $s_\theta = 0$, the EFT operators do not contribute to h_1 decay, and so there is no limit on c_{gg} (the lower band extending across all c_{gg} values). For $s_\theta = 1$, the SM contributions vanish and the observed h_1 production rate is obtained by adjusting c_{gg} (we have only plotted allowed values). For small c_{gg} , we observe the interplay of the mixing and EFT contributions, and larger values of s_θ are allowed than in the $c_{gg} = 0$ limit. In this plot, we retain only the linear contributions in c_{gg} . If the c_{gg}^2 terms become numerically relevant, then the dimension-6 terms must be included in the EFT of Eq. 5.

In Fig. 5, we also fit the h_1 coupling strengths[15] using the 6 parameter fit to the gg initial state at 8 *TeV*,

$$\begin{aligned} \mu_F^{\gamma\gamma} &= 1.13^{+.24}_{-.21} \\ \mu_F^{WW} &= 1.08^{+.22}_{-.19} \\ \mu_F^{ZZ} &= 1.29^{+.29}_{-.25} \\ \mu_F^{bb} &= .66^{+.37}_{-.28} \\ \mu_F^{\tau\tau} &= 1.07^{+.35}_{-.28}. \end{aligned} \quad (21)$$

These are labelled as “h1 95% CL Fits”. The results of the two fits are quite similar.

IV. CONSTRAINTS FROM h_2

We turn now to a joint examination of the measured properties of the h_1 as given in Eq. 21 and the experimental limits on heavy resonances shown in Tabs. I and II for heavy

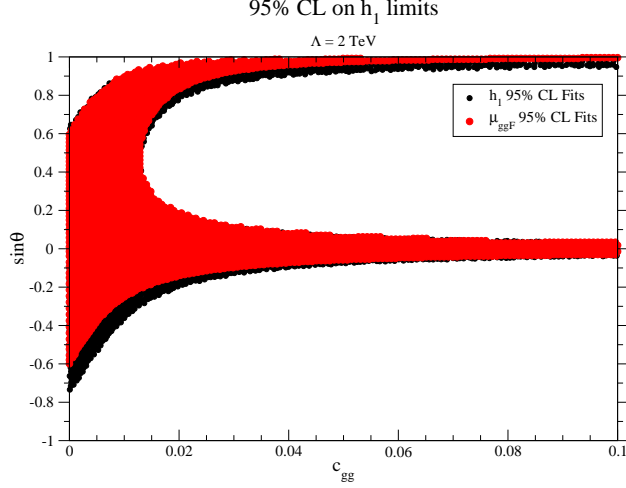


FIG. 5: 95% confidence level allowed regions using the gluon fusion signal strength for h_1 production (red) and allowed regions derived from fits to the signal strengths given in Eq. 21 (black)[15] with $\Lambda = 2 \text{ TeV}$. Only the linear terms in the EFT expansion are included.

Channel	$m_2 = 400 \text{ GeV}$	$m_2 = 600 \text{ GeV}$	$m_2 = 750 \text{ GeV}$
WW	0.362 pb[23]	0.118 pb[23]	0.0361 pb [23]
ZZ	0.0648 pb[24]	0.0218 pb[24]	0.0118 pb[24]
$t\bar{t}$	*	1.2 pb[25]	0.71 pb[25]
$Z\gamma$	0.00720 pb[26]	0.00296 pb[26]	0.00402 pb[26]
$\tau^+\tau^-$	0.087 pb [27]	0.020 pb[27]	0.012 pb[27]
jj	*	3.76 pb[28]	1.79 pb [28]
$h_1 h_1$	0.442 pb[29]	0.137 pb[29]	0.0498 pb [29]
$\gamma\gamma$	0.00215 pb[30]	0.000666 pb[31]	0.00129 pb[30]

TABLE I: 95 % c.l. LHC limits on $\sigma \cdot BR$ for heavy resonances at $\sqrt{S_H} = 8 \text{ TeV}$.

scalars with masses of $m_2 = 400, 600$ and 750 GeV decaying to SM particles using the results of Eq. 11. We calculate the signal rates at leading-order in QCD and normalize to the recommended values for the SM production rates from the LHC Higgs Cross Section Working Group[22] given in Tab. III.

Fig. 6 shows the regions excluded from the the restrictions from resonance searches at 8 TeV and 13 TeV. For $\sin \theta = 0$, there is now an upper limit to c_{gg} that arises from the

Channel	$m_2 = 400$ GeV	$m_2 = 600$ GeV	$m_2 = 750$ GeV
WW	1.4 pb[32]	0.5 pb[32]	0.31 pb[32]
ZZ	0.210 pb[33]	0.083 pb[34]	0.043 pb[34]
$Z\gamma$	0.041 pb[35]	.013 pb[35]	0.010 pb[35]
$\tau^+\tau^-$	0.27 pb[36]	0.053 pb[36]	0.030 pb[36]
jj	*	21.4 pb[37]	9.54 pb[37]
h_1h_1	5.9 pb[38]	1.6 pb[38]	0.85 pb[38]
$\gamma\gamma$	0.0018 pb[39]	0.0015 pb[39]	0.00068 pb[39]
$b\bar{b}$	*	5.1 pb[40]	5.2 pb[40]

TABLE II: 95 % C.L. LHC limits on $\sigma \cdot BR$ for heavy resonances at $\sqrt{S_H} = 13$ GeV.

	8 TeV, $\sigma(pp \rightarrow h_2)$	13 TeV, $\sigma(pp \rightarrow h_2)$
$m_2 = 400$ GeV	3.01 pb	9.52 pb
$m_2 = 600$ GeV	0.52 pb	2.01 pb
$m_2 = 750$ GeV	0.15 pb	0.64 pb

TABLE III: Theoretical cross sections at NNLO+NNLL for heavy scalar resonances from the LHC Higgs Cross Section Working Group[22].

dijet searches. The region at $\sin \theta = 1$, present in the h_1 fits, largely vanishes at $m_2 = 600$ and 750 GeV, and is greatly reduced at $m_2 = 400$ GeV. The excluded region shows little sensitivity to the parameter of the scalar potential. The counting of small parameters is different for the h_2 decays, than in the h_1 case. If we treat both s_θ and c_i as small parameters, then the c_i^2 contributions to h_2 decays are of the same order as the terms independent of the c_i . Hence for the h_2 decays, we include the c_i^2 contributions.

In Fig. 7, we plot the regions allowed by both h_1 coupling fits and resonance searches. We see that the large c_{gg} regions that are allowed by the coupling constant fits are eliminated by the resonance search limits for $m_2 = 600$ GeV and 750 GeV. Considering all constraints, for $m_2 = 600$ and 750 GeV we find $|\sin \theta| \lesssim 0.6$. For $m_2 = 400$ GeV, the resonance searches are less restrictive for positive $\sin \theta$ and the limit is $\sin \theta \gtrsim -0.4$. For all masses these limits

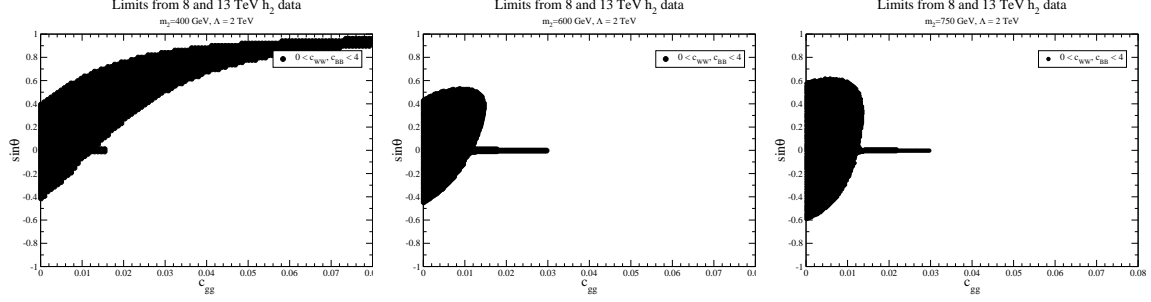


FIG. 6: 95% confidence level allowed regions obtained by varying c_{gg} , c_{WW} , c_{BB} , $\cos\theta$, along with b_1, b_3 and a_2 , allowed by the 8 TeV and 13 TeV resonance searches of Tabs. I and II.

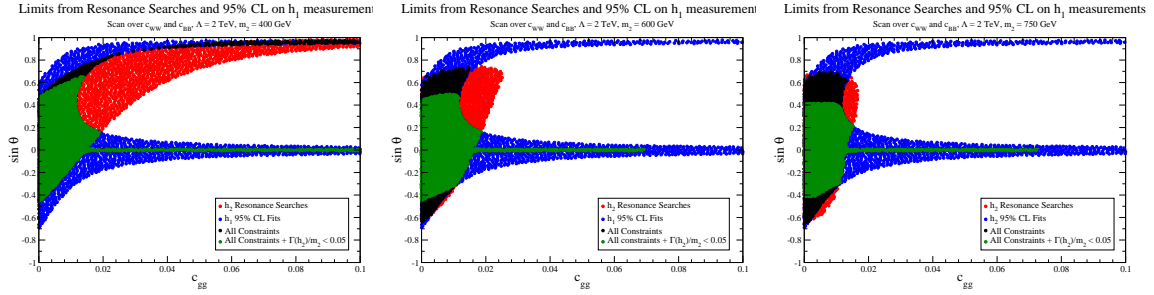


FIG. 7: Allowed regions combining h_1 and h_2 data and a narrow width $\Gamma(h_2)/m_2 < 0.05$ restriction. The new physics scale is set $\Lambda = 2$ TeV, and c_{WW}, c_{BB} are scanned over.

are much weaker than $|\sin\theta| \leq 0.35$ [14] in the renormalizable model without the EFT operators in Eq. 5.

Finally, requiring a narrow width $\Gamma(h_2)/m_2 < 5\%$, where $\Gamma(h_2)$ is the total h_2 width, further constrains the allowed regions of $\sin\theta$. For $m_2 = 600$ and 750 GeV the limit is $|\sin\theta| \lesssim 0.4$. For $m_2 = 400$ GeV, the effect of the the narrow width restriction is to eliminate the large $\sin\theta \sim 1$ region. The remaining parameter region is $-0.4 \lesssim \sin\theta \lesssim 0.7$.

V. CONCLUSIONS

We examined the effects on Higgs physics of a gauge singlet scalar which mixes with the SM-like 125 GeV Higgs boson when the theory is augmented by EFT operators coupling the singlet scalar to SM gauge bosons. The new feature of our analysis is a study of the properties of both the 125 GeV and heavy scalar resonance, and the demonstration that significant cancellations are possible between effects in the two sectors. We fit our model parameters to

the 7 and 8 TeV combined ATLAS and CMS precision Higgs measurements [15] and applied constraints from scalar resonance searches at the 8 and 13 TeV LHC.

We find that the inclusion of the operators greatly changes the allowed values of the scalar mixing angle. In the renormalizable model, the strongest bound from Higgs precision is $|\sin\theta| \leq 0.35$ [14]. Including the EFT operators between the singlet scalar and SM gauge bosons, we find Higgs precision measurements and scalar resonance searches give $\sin\theta \gtrsim -0.4$ for a heavy scalar mass of 400 GeV and $|\sin\theta| \lesssim 0.6$ for masses of 600 and 750 GeV. If the additional requirement of a narrow width $\Gamma(h_2)/m_2 < 0.05$ is included, the limits are $-0.4 \lesssim \sin\theta \lesssim 0.7$ for a heavy scalar mass of 400 GeV and $|\sin\theta| \lesssim 0.4$ for masses of 600 and 750 GeV. In all cases, these restrictions are less than those in the renormalizable theory.

Acknowledgements

This work is supported by the U.S. Department of Energy under grant de-sc0012704. We thank Chien-Yi Chen for many valuable discussions about the singlet model. Digital data related to our results can be found at *quark.phy.bnl.gov/Digital_Data_Archive/dawson/singlet_16*.

-
- [1] Jose R. Espinosa, Thomas Konstandin, and Francesco Riva. Strong Electroweak Phase Transitions in the Standard Model with a Singlet. *Nucl.Phys.*, B854:592–630, 2012, 1107.5441.
 - [2] Stefano Profumo, Michael J. Ramsey-Musolf, and Gabe Shaughnessy. Singlet Higgs phenomenology and the electroweak phase transition. *JHEP*, 0708:010, 2007, 0705.2425.
 - [3] Stefano Profumo, Michael J. Ramsey-Musolf, Carroll L. Wainwright, and Peter Winslow. Singlet-catalyzed electroweak phase transitions and precision Higgs boson studies. *Phys. Rev.*, D91(3):035018, 2015, 1407.5342.
 - [4] David Curtin, Patrick Meade, and Chiu-Tien Yu. Testing Electroweak Baryogenesis with Future Colliders. 2014, 1409.0005.
 - [5] Maxim Perelstein and Yu-Dai Tsai. 750 GeV Di-photon Excess and Strongly First-Order Electroweak Phase Transition. 2016, 1603.04488.
 - [6] Donal O’Connell, Michael J. Ramsey-Musolf, and Mark B. Wise. Minimal Extension of the Standard Model Scalar Sector. *Phys.Rev.*, D75:037701, 2007, hep-ph/0611014.
 - [7] Vernon Barger, Paul Langacker, Mathew McCaskey, Michael Ramsey-Musolf, and Gabe Shaughnessy. Complex Singlet Extension of the Standard Model. *Phys.Rev.*, D79:015018, 2009, 0811.0393.
 - [8] Giovanni Marco Pruna and Tania Robens. The Higgs Singlet extension parameter space in the light of the LHC discovery. *Phys.Rev.*, D88:115012, 2013, 1303.1150.
 - [9] Chien-Yi Chen, S. Dawson, and I. M. Lewis. Exploring resonant di-Higgs boson production in the Higgs singlet model. *Phys. Rev.*, D91(3):035015, 2015, 1410.5488.
 - [10] Tania Robens and Tim Stefaniak. LHC Benchmark Scenarios for the Real Higgs Singlet Extension of the Standard Model. 2016, 1601.07880.
 - [11] S. Dawson and I. M. Lewis. NLO corrections to double Higgs boson production in the Higgs singlet model. *Phys. Rev.*, D92(9):094023, 2015, 1508.05397.
 - [12] Raul Costa, Margarete Mhleitner, Marco O. P. Sampaio, and Rui Santos. Singlet Extensions of the Standard Model at LHC Run 2: Benchmarks and Comparison with the NMSSM. 2015, 1512.05355.
 - [13] Amine Ahriche. What is the criterion for a strong first order electroweak phase transition in singlet models? *Phys.Rev.*, D75:083522, 2007, hep-ph/0701192.

- [14] Georges Aad et al. Constraints on new phenomena via Higgs boson couplings and invisible decays with the ATLAS detector. *JHEP*, 11:206, 2015, 1509.00672.
- [15] Measurements of the Higgs boson production and decay rates and constraints on its couplings from a combined ATLAS and CMS analysis of the LHC pp collision data at $\sqrt{s} = 7$ and 8 TeV. Technical Report ATLAS-CONF-2015-044, CERN, Geneva, Sep 2015.
- [16] Sally Dawson and Wenbin Yan. Hiding the Higgs Boson with Multiple Scalars. *Phys.Rev.*, D79:095002, 2009, 0904.2005.
- [17] Martin Bauer, Anja Butter, Juan Gonzalez-Fraile, Tilman Plehn, and Michael Rauch. Learning from the New Higgs-like Scalar before It Vanishes. 2016, 1607.04562.
- [18] Kingman Cheung, P. Ko, Jae Sik Lee, Jubin Park, and Po-Yan Tseng. Double Higgscision: 125 GeV Higgs boson and a potential diphoton Resonance. 2016, 1608.00382.
- [19] John F. Gunion, Howard E. Haber, Gordon L. Kane, and Sally Dawson. The Higgs Hunter’s Guide. *Front. Phys.*, 80:1–448, 2000.
- [20] Abdelhak Djouadi. The Anatomy of electro-weak symmetry breaking. I: The Higgs boson in the standard model. *Phys. Rept.*, 457:1–216, 2008, hep-ph/0503172.
- [21] Roberto Contino, Margherita Ghezzi, Christophe Grojean, Margarete Mhlleitner, and Michael Spira. eHDECAY: an Implementation of the Higgs Effective Lagrangian into HDECAY. *Comput. Phys. Commun.*, 185:3412–3423, 2014, 1403.3381.
- [22] LHC Higgs Cross Section Working Group, S. Heinemeyer, C. Mariotti, G. Passarino, and R. Tanaka (Eds.). Handbook of LHC Higgs Cross Sections: 3. Higgs Properties. *CERN-2013-004*, CERN, Geneva, 2013, 1307.1347.
- [23] Georges Aad et al. Search for a high-mass Higgs boson decaying to a W boson pair in pp collisions at $\sqrt{s} = 8$ TeV with the ATLAS detector. *JHEP*, 01:032, 2016, 1509.00389.
- [24] Georges Aad et al. Search for an additional, heavy Higgs boson in the $H \rightarrow ZZ$ decay channel at $\sqrt{s} = 8$ TeV in pp collision data with the ATLAS detector. *Eur. Phys. J.*, C76(1):45, 2016, 1507.05930.
- [25] Georges Aad et al. A search for $t\bar{t}$ resonances using lepton-plus-jets events in proton-proton collisions at $\sqrt{s} = 8$ TeV with the ATLAS detector. *JHEP*, 08:148, 2015, 1505.07018.
- [26] Georges Aad et al. Search for new resonances in $W\gamma$ and $Z\gamma$ final states in pp collisions at $\sqrt{s} = 8$ TeV with the ATLAS detector. *Phys. Lett.*, B738:428–447, 2014, 1407.8150.
- [27] Georges Aad et al. Search for neutral Higgs bosons of the minimal supersymmetric stan-

- dard model in pp collisions at $\sqrt{s} = 8$ TeV with the ATLAS detector. *JHEP*, 11:056, 2014, 1409.6064.
- [28] Vardan Khachatryan et al. Search for narrow resonances in dijet final states at $\sqrt{s}=8$ TeV with the novel CMS technique of data scouting. 2016, 1604.08907.
 - [29] Vardan Khachatryan et al. Search for resonant pair production of Higgs bosons decaying to two bottom quark?antiquark pairs in proton?proton collisions at 8 TeV. *Phys. Lett.*, B749:560–582, 2015, 1503.04114.
 - [30] Vardan Khachatryan et al. Search for diphoton resonances in the mass range from 150 to 850 GeV in pp collisions at $\sqrt{s} = 8$ TeV. *Phys. Lett.*, B750:494–519, 2015, 1506.02301.
 - [31] Georges Aad et al. Search for Scalar Diphoton Resonances in the Mass Range 65 – 600 GeV with the ATLAS Detector in pp Collision Data at $\sqrt{s} = 8$ TeV. *Phys. Rev. Lett.*, 113(17):171801, 2014, 1407.6583.
 - [32] Search for a high-mass Higgs boson decaying to a pair of W bosons in pp collisions at $\sqrt{s}=13$ TeV with the ATLAS detector. Technical Report ATLAS-CONF-2016-074, CERN, Geneva, Aug 2016.
 - [33] Measurements of properties of the Higgs boson and search for an additional resonance in the four-lepton final state at $\sqrt{s} = 13$ TeV. Technical Report CMS-PAS-HIG-16-033, CERN, Geneva, 2016.
 - [34] Search for new phenomena in the $Z(\rightarrow \ell\ell) + E_{\text{T}}^{\text{miss}}$ final state at $\sqrt{s} = 13$ TeV with the ATLAS detector. Technical Report ATLAS-CONF-2016-056, CERN, Geneva, Aug 2016.
 - [35] Search for new resonances decaying to a Z boson and a photon in 13.3 fb $^{-1}$ of pp collisions at $\sqrt{s} = 13$ TeV with the ATLAS detector. Technical Report ATLAS-CONF-2016-044, CERN, Geneva, Aug 2016.
 - [36] Search for Minimal Supersymmetric Standard Model Higgs Bosons H/A in the $\tau\tau$ final state in up to 13.3 fb $^{-1}$ of pp collisions at $\sqrt{s}= 13$ TeV with the ATLAS Detector. Technical Report ATLAS-CONF-2016-085, CERN, Geneva, Aug 2016.
 - [37] Searches for narrow resonances decaying to dijets in proton-proton collisions at 13 TeV using 12.9 inverse femtobarns. Technical Report CMS-PAS-EXO-16-032, CERN, Geneva, 2016.
 - [38] Search for resonant Higgs boson pair production in the $b\bar{b}\tau^+\tau^-$ final state using 2016 data. Technical Report CMS-PAS-HIG-16-029, CERN, Geneva, 2016.
 - [39] Search for scalar diphoton resonances with 15.4 fb $^{-1}$ of data collected at $\sqrt{s}=13$ TeV in

2015 and 2016 with the ATLAS detector. Technical Report ATLAS-CONF-2016-059, CERN, Geneva, Aug 2016.

- [40] Search for a narrow heavy decaying to bottom quark pairs in the 13 TeV data sample. Technical Report CMS-PAS-HIG-16-025, CERN, Geneva, 2016.